Journal of Molecular and Cellular Cardiology 204 (2025) 79–88

Contents lists available at ScienceDirect

Journal of Molecular and Cellular Cardiology

journal homepage: www.elsevier.com/locate/yjmcc

The role of connexin-43 in modeling arrhythmogenic diseases with induced pluripotent stem cell-derived cardiomyocytes

Xijian Ke [a,b], Jonathan S. Baillie [c], Enrico D. Lemma [d,e,f], Martin Bastmeyer [d,g,h,i], Markus Hecker [a,j], Nina D. Ullrich [a,c,i,j,*]

[a] Department of Physiology and Pathophysiology, Division of Cardiovascular Physiology, Heidelberg University, 69120 Heidelberg, Germany
[b] Department of Anesthesiology and Pain Medicine, Tongji Hospital, Tongji Medical College, Huazhong University of Science and Technology, 430030 Wuhan, China
[c] Department of Physiology, University of Bern, Buehlplatz 5, 3012 Bern, Switzerland
[d] Zoological Institute, Cell and Neurobiology, Karlsruhe Institute of Technology (KIT), Fritz-Haber-Weg 4, 76131, Karlsruhe, Germany
[e] Department of Engineering, Università Campus Bio-Medico di Roma, via Álvaro del Portillo 21, 00128 Rome, Italy
[f] Institute of Nanotechnology (NANOTEC), National Research Council, via Monteroni, 73100 Lecce, Italy
[g] Institute of Applied Physics, Karlsruhe Institute of Technology (KIT), Wolfgang-Gaede-Strasse 1, 76131 Karlsruhe, Germany
[h] Institute of Functional Interfaces (IFG), Karlsruhe Institute of Technology (KIT), Hermann-von-Helmholtz-Platz 1, 76344 Eggenstein-Leopoldshafen, Germany
[i] Heidelberg-Karlsruhe Research Partnership (HEiKA), Research Bridge (Synthetic Biology), Heidelberg University and Karlsruhe Institute of Technology, Germany
[j] DZHK (German Center for Cardiovascular Research), Partner Site Heidelberg/Mannheim, University of Heidelberg, Heidelberg, Germany

ARTICLE INFO

Keywords:
Arrhythmogenic disease
Gap junctions
Cx43
$Na_v1.5$
microRNA-1
iPSC-cardiomyocytes
Patch clamp

ABSTRACT

A common pathophysiological characteristic of arrhythmic diseases is the disruption of electrical signal transmission across the heart causing life-threatening rhythm disorders. These conditions are associated with decreased expression of connexin-43 (Cx43) at intercalated discs and its translocation to the lateral membranes, however, the underlying mechanisms remain unclear. Induced pluripotent stem cell-derived cardiomyocytes (iPSC-CM) offer a model for studying these pathophysiological processes. Here, we tested the hypothesis that chronic stress, usually preceding arrhythmic developments, modulates Cx43 expression. iPSC-CM were electrically stimulated at a normal rate and by tachypacing, and their electrical and Ca^{2+} signaling properties were analyzed. Our data revealed that tachypacing significantly reduced Cx43 expression by a micro-RNA miR-1-dependent mechanism. Anti-miR-1 treatment restored Cx43 expression in conditions of stress, enhanced Na^{+} currents, improved Ca^{2+} propagation and synchronized electrical activity. These findings suggest miR-1 as a potential pharmacological target for mitigating arrhythmogenic remodeling and restoring robust electrical signal transmission in cardiomyocytes.

1. Introduction

Arrhythmogenic disorders are characterized by abnormalities in the electrical conduction system of the heart, leading to disruption of the spatiotemporally synchronized excitation and contraction pattern. While arrhythmogenic cardiomyopathies often result from genetic mutations affecting structural proteins or voltage-dependent ion channel function, non-genetic conduction defects include a range of cardiac conditions that are influenced by various environmental, physiological or pathological factors. These conditions may arise due to electrolyte imbalances, ischemic settings or age-related changes leading to arrhythmias such as atrial fibrillation, ventricular tachycardia or bradyarrhythmia. Myocardial infarction is a primary cause of non-inherited arrhythmias with pathological tissue remodeling leading to cardiomyocyte damage and cell death, followed by scar formation [1]. Fibrosis disrupts normal conduction pathways, creating re-entrant circuits that predispose individuals to premature life-threatening arrhythmias [2].

A common hallmark of arrhythmogenic disorders is structural and functional changes at the cardiomyocyte level, particularly regarding the intercellular connections consisting of gap junctions. Gap junctions are specialized membrane channels that enable direct electrical and metabolic coupling between adjacent cells. They facilitate the rapid propagation of action potentials (AP) across cardiomyocytes, ensuring efficient electrical coupling and synchronous contraction [3]. In healthy ventricular cardiomyocytes, connexin 43 (Cx43) is the most prevalent

* Corresponding author at: University of Bern, Department of Physiology, Buehlplatz 5, 3012 Bern, Switzerland.
E-mail address: nina.ullrich@unibe.ch (N.D. Ullrich).

https://doi.org/10.1016/j.yjmcc.2025.05.008
Received 6 January 2025; Received in revised form 20 May 2025; Accepted 23 May 2025
Available online 26 May 2025

gap junction protein. It is preferentially localized within the intercalated discs (ICD), forming hexameric assemblies called hemichannels or connexons, which can dock with connexons of adjacent cells to create gap junction channels [4,5]. Both, hemichannels and gap junctions, allow the passage of ions and small molecules, which in the case of intercellular gap junction channels will directly connect one cell to another, enabling metabolic and electrical coupling of cardiomyocytes and the establishment of a functional syncytium. Altered expression levels and displacement of Cx43 from the ICD to the lateral membranes may result in enhanced hemichannel presence and leads to impaired gap junction function resulting in reduced conduction velocity, increased electrical signal dispersion and delayed repolarization, thereby leading to the formation of an arrhythmogenic substrate [3,6–8].

Small non-coding RNA molecules (micro- or miRNAs) are powerful tools in the regulation of normal cell function and development as they play a crucial role in regulating and controlling gene expression. Moreover, dysregulation of miRNAs has been linked to various problems, including cardiovascular diseases. The miRNA miR-1 plays a significant role in the modulation of Cx43 expression post-transcriptionally by binding to the 3′ untranslated region of Cx43 mRNA, leading to its degradation or translational repression [9,10]. It has been implicated in many cardiac diseases, including ischemic-reperfusion injury, arrhythmia and heart failure [11,12]. miR-1 regulates the abundance and distribution of Cx43 channels, thereby influencing intercellular communication and electrical signal propagation in the heart. Studies revealed that miR-1 exerts post-transcriptional control over Cx43 expression, thereby influencing cardiac conduction and electrical synchronization [13]. The significance of this molecular axis in cardiac function and disease progression is further highlighted by the reciprocal regulation between miR-1 and Cx43, which reveals a complex interplay governing cardiac electrical coupling and rhythmogenesis. Conversely, Cx43 can also influence miR-1 expression through complex signaling pathways. Studies have shown that altered Cx43 expression or function may affect the expression of miR-1 and its target genes, establishing a feedback loop that further modulates cardiac electrophysiology and rhythmogenesis [14,15].

Previously, we characterized the function of Cx43 and the impact of chronic stress and miR-1 on the control of Cx43 expression in induced pluripotent stem cell-derived cardiomyocytes (iPSC-CM), which represent the novel standard model to study the molecular basis of cardiac diseases in vitro [14,16–19]. In this study, we used iPSC-CM as a model for arrhythmogenic diseases. We tested the hypothesis that the negative effect of chronic cell stress on Cx43 expression and electrical signal propagation can be reversed by reducing miR-1 activity. The aim of this study was to identify key molecular players involved in the regulation of Cx43 expression and to restore robust electrical signal propagation during phases of increased stress.

2. Experimental procedures

Please consult the Supplemental information for detailed description of the experimental procedures.

2.1. Cell culture

Murine atrial HL-1 cardiomyocytes were used as a control cell line to test and establish new protocols and techniques. HL-1 cells were cultured and passaged to maintain their cardiac phenotype following previously published protocols [20].

Murine induced pluripotent stem cell-derived cardiomyocytes (iPSC-CM, Cor.At CL-1 cardiomyocytes, commercially available from Ncardia®, Cologne, Germany) derived from transgenic mice were acquired and 15 batches of differentiated cells were used for this study, considered as 15 biological replicates. Each replicate contained 10^6 cells and was used for experiments for one month. For further information, please see the Supplemental methods.

2.2. Direct microcontact printing

To grow cells in specific patterns (e.g. to produce cell strands), we applied the direct micro-contact printing technique (μCP) modified from Singhvi et al. [21] with additional passivation. PDMS stamps production and the stamping procedure are detailed in the Supplemental methods and illustrated in the Supplemental Fig. 1.

2.3. Electrical tachypacing

An electric field stimulator (SIU-102B stimulus isolation unit, MCS GmbH) was connected to a pulse generator (homemade, Heidelberg University) and to pairs of carbon electrodes that were placed into the cell culture dishes. Cells were paced during culture inside the incubator. A series of 30-V bipolar square-wave stimulation pulses with different frequencies was generated. In μCP experiments, the electric field direction was aligned to the long axis of the cell streets. To prevent cell detachment during long-term electric pacing, we used homemade lumox foil dishes (Sarstedt) instead of glass-bottom dishes.

2.4. Transfection of anti-miR-1 oligonucleotides

To study the effect of miR-1 inhibition on Cx43 expression, we used a phosphorothioate-modified, 5′-fluorescein-labelled power inhibitor against mature miR-1 (named anti-miR-1): mmu-miR-1a-3p miRCURY LNA power miRNA inhibitor (Exiqon, 4100839-111, Denmark). The base sequence is as follows: 5′-ACATACTTCTTTACATTCCA-3′. Scrambled RNA (Exiqon, Denmark) with a base sequence of 5′-TAACACGTCTATACGCCCA-3′ was used as the negative control. A final concentration of 50 nM anti-miR-1 was diluted in cell culture medium and added to iPSC-CM without any assisting transfection reagents. Culture medium was changed after 24 h. Transfection efficiency was monitored daily by checking the 6-FAM fluorescent signal expression (Supplemental Fig. 2). Cells were used for functional experiments or immunostainings 72 h after transfection.

2.5. Immunocytochemistry and quantification of Cx43

Immunocytochemistry and laser-scanning confocal imaging were used to estimate the expression of Cx43. For detailed information, please see the Supplemental methods.

In Fiji/ImageJ, after “grey-scale” processing of the Cx43 channel, we used “max entropy” to set the threshold and filter the Cx43 signals as previously published [18]. Then free-hand lines were drawn along the cell border to define the cell border area. The area occupation ratio of Cx43 clusters in the cell-cell contact border was calculated in the ROI manager. Accordingly, we wrote a macro-based plugin to process all the image data universally.

2.6. Ca^{2+} imaging and Ca^{2+} transient propagation

To investigate Ca^{2+} transient propagation, iPSC-CM were incubated with 2 μM fluo-4 AM (F14201, Life Technologies GmbH, Darmstadt, Germany) in Tyrode’s solution for 20 min at room temperature followed by deesterification. Linescan images were taken on a confocal microscope to record Ca^{2+} transients at high temporal resolution. The composition of the Tyrode’s solution is listed in Supplementary Table 1, and detailed technical information is provided in the Supplemental methods.

2.7. Electrophysiology: multi-electrode arrays (MEA)

The electrical activity of iPSC-CM was recorded using 6-well-MEA dishes consisting of 6 isolated chambers. Each chamber has nine recording electrodes and one reference electrode (MCS, Reutlingen, Germany). The spontaneous electrical activity was monitored and

recorded on all electrodes simultaneously. The frequency of spontaneous electrical activity and the inter-spike intervals were analyzed with the MC-Rack software and further processed in OriginPro. Detailed information is given in the Supplemental file.

2.8. Patch-clamp: whole-cell voltage and current clamp techniques

Voltage- and current-clamp recordings were based on a standard whole-cell recording technique. [22] A HEKA EPC-10-USB amplifier (HEKA Elektronik, Germany) controlled by the Patchmaster software was used and combined with an inverted Olympus LSCM as described above. Healthy and single iPSC-CM were selected and patch-clamped using the classical voltage-clamp technique. Patchmaster software was used for stimulation and data acquisition. The contents of the bath and pipette solutions (internal solution) are shown in Supplementary Table 2. For AP recordings, iPSC-CM were patched in the current-clamp mode using bath and pipette solutions as listed in Supplementary Table 3. Details of the voltage-clamp and current-clamp protocols can be found in the Supplemental methods file.

2.9. Statistical analysis

OriginPro 2023 software was used for data analysis, statistical evaluation, and graphical data display. Fiji/ImageJ was used for image data extraction and analysis. Data are presented as mean ± SEM or mean ± SD as indicated. Experiments were repeated n-times from at least 3 different replicates of cells (N); n indicates the number of measured cells or cell preparations as indicated in the figure legends. For comparing two groups, the Student's *t*-test was applied after a test for homogeneity of variance. At $p < 0.05$, data groups were assumed to be significantly different.

3. Results

3.1. Production of cell streets using the μCP technique

To investigate Cx43 expression patterns, we designed a specific growth pattern to analyze intercellular coupling and electrical signal propagation under different conditions at the cellular level in HL-1 cells and iPSC-CM. Monolayer culture signal propagation disperses along the pathway of least resistance. Therefore, signal spreading is best studied in thin rows of cells to avoid non-linear propagation. Using the direct μCP technique, cells were grown along a thin line pattern of extracellular matrix protein (ECM)-coated area (Fig. 1A). HL-1 cells were used to establish the technique and to optimize the conditions for patterned growth (Fig. 1Aa, c). Cell adherence followed the printed pattern of ECM forming thin cell streets of 400 μm length and 25 μm width. The same protocol was then applied to iPSC-CM (Fig. 1Ab, d). The detailed view in Fig. 1Ad demonstrates alignment of iPSC-CM according to the long axis of the printing pattern and elongation of single cells within the cell street. In this growth configuration, structural and functional properties of intercellular communication were investigated and characterized at different conditions of cell stress.

3.2. Characterization of Cx43 expression in chronically stressed iPSC-CM

To induce chronic stress as a model for arrhythmogenic diseases, we triggered cell stress and cellular remodeling in vitro as previously described [14]. Chronic tachypacing was induced by field stimulation at 4 Hz on cell strands of iPSC-CM to elicit pathological gap junction remodeling. Immunocytochemical staining and confocal imaging were used to assess changes in the sarcolemmal expression pattern of Cx43 under different conditions. Three experimental groups were designed to investigate the effect of tachypacing on Cx43 expression: non-pacing (but spontaneous activity), tachypacing at 4 Hz including scramble miRNA, and tachypacing with inhibition of miR-1 using anti-miR-1. Fig. 1B shows representative images of the Cx43 distribution at the sarcolemma in non-paced (a) and tachypaced (b) iPSC-CM grown in cell strands. Dot-like Cx43 clusters were detected at the cell boundaries, in particular at the cell-cell contact sites. Chronic tachypacing of 72 h led to significant reduction in sarcolemmal Cx43 expression compared to non-paced control cells. According to our previously published data, chronic tachypacing and cell stress lead to an increase in miR-1, which reduces Cx43 expression [14]. Therefore, inhibition of miR-1 during chronic tachypacing may prevent Cx43 remodeling and the loss of sarcolemmal expression. The images in Fig. 1Bc show representative images of Cx43 expression after 72 h of tachypacing in the presence of the miR-1 inhibitor anti-miR-1. Quantification of Cx43 expression was done by measuring the Cx43 cluster occupation ratio against the cell border to represent the relative expression level of Cx43 at the sarcolemma. Data were collected using a self-written macro in ImageJ and are summarized in Fig. 1C. For the control group, the Cx43 cluster area occupation ratio

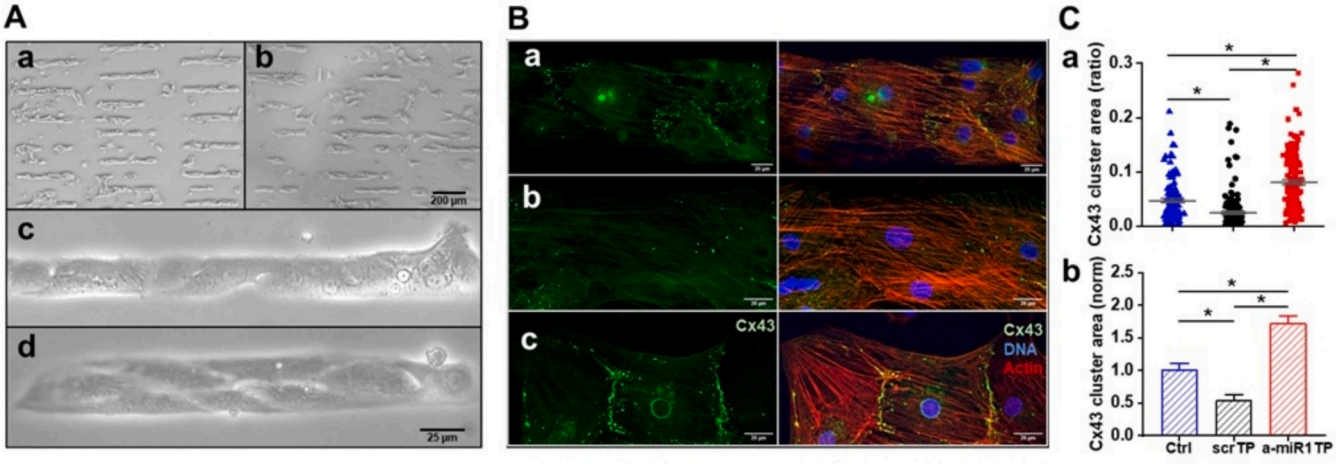

Fig. 1. Effect of tachypacing and miR-1 inhibition on Cx43 expression in μCP cell strands. (A) Overview of HL-1 cells (a, c) and iPSC-CM (b, d) seeded on μCP streets (after 48 h). (B) Representative images of Cx43 expression in iPSC-CM cell strands: (a) control; (b) tachypacing (TP with scramble miR); (c) miR-1 inhibition during tachypacing (a-miR TP). Green: Cx43; red: F-actin; blue: nucleus counterstained with DAPI, scale bar: 20 μm. (C, a) Quantification of the occupation ratio of Cx43 cluster area at the membrane and (b) normalization of scramble TP ($n = 153$) and a-miR1-TP ($n = 168$) to the control group ($n = 129$); n indicates the number of clusters. One-way ANOVA showed that the Cx43 cluster area occupation ratio in different groups was significant; Tukey test was used to compare the means. * indicates significant differences at $p < 0.05$. (For interpretation of the references to color in this figure legend, the reader is referred to the web version of this article.)

was 4.7 ± 0.34 % (mean ± SEM, n = 129 clusters); for the chronic tachypacing plus control oligonucleotide treatment group (scr-TP), the Cx43 cluster area occupation ratio was 2.5 ± 0.27 % (n = 153); and for the tachypacing plus anti-miR-1 treatment group, the Cx43 cluster area occupation ratio was 8.1 ± 0.39 % (n = 168). All data were normalized to the control group as shown in Fig. 1Cb. One-way ANOVA showed that the Cx43 cluster area occupation ratio was significantly different in the test groups; Tukey post-hoc test was used to compare the means. The results demonstrate that the Cx43 cluster area in the cell border was significantly decreased by chronic tachypacing, but inhibition of miR-1 preserved Cx43 expression, resulting in enhanced localization of Cx43 at the sarcolemma even under tachypacing conditions.

3.3. Inhibition of miR-1 significantly enhanced Ca^{2+} wave propagation across iPSC-CM

We first investigated Ca^{2+} transient propagation across a monolayer of HL-1 cells, which is transmitted by intercellular coupling. Cells were loaded with the Ca^{2+}-sensitive fluorescent indicator fluo-4 and imaged using either epi-fluorescence microscopy or laser-scanning confocal microscopy. The direction and speed of propagation remained unchanged for a certain period. Along the direction of propagation, a linescan was set to record details of the spatiotemporal properties of the Ca^{2+} transients and their propagation across several cells, as shown in Fig. 2A. The areas of measurement were randomly selected within the same dish. The propagation velocity of Ca^{2+} transients in HL-1 monolayers corresponded to 1.7 ± 0.1 μm/ms (mean ± SEM, n = 22; Fig. 2B, C).

We used the same strategy to calculate the Ca^{2+} transient propagation velocity in a monolayer of iPSC-CM. In iPSC-CM, transfection with anti-miR-1 significantly increased the Ca^{2+} transient propagation velocity compared to the scramble-miR-treated control cells (62.8 ± 4.4 vs. 49.1 ± 4.7 μm/ms, mean ± SEM; Fig. 2D). One-way ANOVA and Tukey test confirmed a significant difference in the Ca^{2+} transient propagation velocity. These data demonstrate not only that the propagation velocity of Ca^{2+} transients across iPSC-CM cells was an order of magnitude faster than in HL-1. Moreover, miR-1 inhibition significantly accelerated Ca^{2+} transient propagation in iPSC-CM. We also investigated the Ca^{2+} transient propagation in cell strands of iPSC-CM. The propagation velocity of Ca^{2+} transients amounted to 31.6 ± 2.7 μm/ms in anti-miR-1 transfected cell strands vs. 29.2 ± 3.7 μm/ms in control (mean ± SEM) demonstrating a tendency toward a higher propagation velocity in anti-miR-1-treated cells vs. control, however, the difference was not significant (Supplemental Fig. 3).

The specificity of gap junction-dependent cell coupling and Ca^{2+} transient propagation was demonstrated in two separate experiments involving cell pairs. Supplemental Fig. 4 illustrates dye coupling in cell pairs using calcein under control conditions and in presence of the gap junction uncoupler heptanol (1 mM). Using a patch clamp pipette, calcein was injected into *Cell 1* of a cell pair. In dependence of the presence and function of gap junctional coupling, calcein diffused into *Cell 2*. The data demonstrate that fluorescence in *Cell 2* progressively increased in function of time. Inhibition of gap junction function efficiently prevented dye diffusion. Furthermore, upon electrical stimulation, the Ca^{2+} transient propagation from one cell to its coupled neighbor was measured at control and during administration of heptanol (Supplemental Fig. 5). These experiments demonstrate that electrical uncoupling of cell pairs significantly decreased Ca^{2+} transient propagation. Uncoupling leads to a strong drop in amplitudes and significant slowing of the upstroke velocity of the Ca^{2+} transient in *Cell 2*, demonstrating the need of gap junctional coupling for electrical and Ca^{2+} signal transmission between iPSC-CM.

Next, the rhythmicity of the Ca^{2+} transients was investigated in iPSC-CM. Fig. 3A displays representative linescan images of Ca^{2+} transients and their corresponding line profiles. Cells transfected with anti-miR-1 presented more regular and frequent Ca^{2+} transients. Compared with control scramble oligonucleotide-treated iPSC-CM, anti-miR-1-treated cells demonstrated significantly shorter time intervals between single Ca^{2+} transients (1492 ± 111 ms in control vs. 1113 ± 36 ms in anti-miR-1, mean ± SEM), and significantly lower variability of the time interval between the Ca^{2+} transients (coefficient of variation (CoV): 0.95 ± 0.11 in control vs. 0.34 ± 0.03 in anti-miR-1, respectively). Similarly, anti-miR-1-treated iPSC-CM had a significantly higher frequency of Ca^{2+} transients (0.7 ± 0.05 Hz in control vs. 0.9 ± 0.03 Hz in anti-miR-1, Fig. 3B) with lower CoV of frequency (0.37 ± 0.03 in control vs. 0.27 ± 0.02 in anti-miR-1). These experiments demonstrate that miR-1 inhibition significantly enhanced Ca^{2+} transient propagation in iPSC-CM, indicating improved intercellular coupling and increased cell excitability due to elevated Cx43 expression.

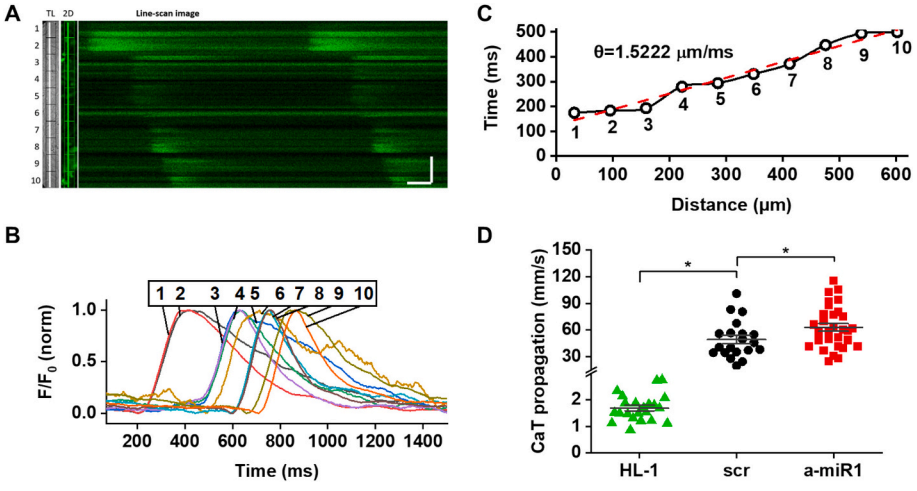

Fig. 2. Effect of miR-1 inhibition on Ca^{2+} transients in HL-1 cells and iPSC-CM. (A) Transmission light image of HL-1 cells (TL, left), fluorescence image (2D, middle), and the corresponding linescan image (right). The scanning line was evenly divided into ten segments as indicated; vertical scale bar = 100 μm; horizontal scale bar = 200 ms. (B) The Ca^{2+} transient profiles of each segment are shown. Note: the fluorescence intensity of the Ca^{2+} transient was smoothed and normalized to 0–1 to facilitate comparison. (C) The activation time point of each segment was plotted against distance. The reciprocal of slope (θ) from a linear fit (red dashed line) was determined as the mean propagation velocity. (D) Comparison of Ca^{2+} transient propagation velocity among monolayers of HL-1 cells (n = 22), control (n = 20) and anti-miR-1 oligonucleotide-treated iPSC-CM (n = 30). Statistical difference was tested using one-way ANOVA; * indicates significant difference at $p < 0.05$. (For interpretation of the references to color in this figure legend, the reader is referred to the web version of this article.)

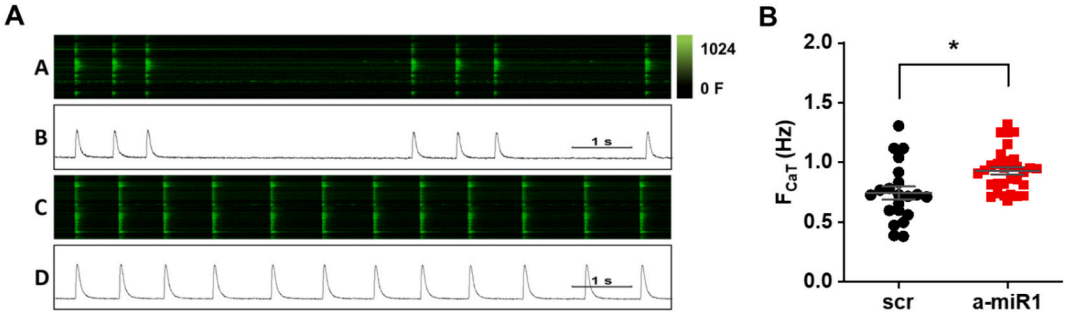

Fig. 3. Effect of miR-1 inhibition on frequency and rhythmicity of Ca^{2+} transients in iPSC-CM. (A) Linescan images and line profiles of Ca^{2+} transients in iPSC-CM monolayers transfected with the control oligonucleotide (a, b) and anti-miR-1 (c, d). (B) Ca^{2+} transient frequency of control scramble ($n = 21$) and anti-miR-1 transfected iPSC-CM ($n = 31$). Statistical difference was tested using Student's *t*-test; * indicates significance at $p < 0.05$.

3.4. Inhibition of miR-1 significantly increased the voltage-dependent sodium current

Using the whole-cell mode of the patch-clamp technique, we studied the functional effects of anti-miR-1 oligonucleotide treatment on the voltage-gated sodium current (I_{Na}) in single iPSC-CM. Immunostainings confirmed $Na_v1.5$ channel expression in next vicinity of Cx43 expression at the cell-cell borders (Supplemental Fig. 6). We first validated the specificity of I_{Na} recordings by a tetracaine-mediated Na^+ channel block in single iPSC-CM. CsCl, $CdCl_2$, and $BaCl_2$ salts were added to the bath solution to block K^+ and Ca^{2+} currents. After fast and slow compensation, starting from a holding potential of −80 mV, a 1-step protocol was executed to elicit maximal I_{Na} at −20 mV in the voltage-clamp mode. Tetracaine was administered by local perfusion close to the target cell. I_{Na} was completely blocked by 1 mM tetracaine in Tyrode's solution (Supplemental Fig. 7).

Traces of the "step families" of I_{Na} for control- or anti-miR-1-transfected cells are illustrated (Fig. 4A and B). Holding potential of all voltage-clamp recordings was set to −80 mV. I_{Na} of each cell was normalized to its membrane capacitance (i.e., current density). The current density was then plotted against the corresponding voltage of the test pulse to create the current-voltage (I-V) relationship (Fig. 4C). The I-V curve of I_{Na} resembles an inverted bell shape in the range of −60 mV to +30 mV, with the peak located near −30 mV and −20 mV, and the activation threshold potential was located between −60 mV and −50 mV. Between −20 mV and +30 mV, the I-V relationship was approximately linear. These results demonstrate that the I_{Na} density of iPSC-CM in the presence of the miR-1 inhibitor was significantly increased compared with control (control: 12.3 ± 1.3 pA/pF vs. anti-miR-1: 19.5 ± 2.6 pA/pF; Fig. 4D), indicating the presence of more

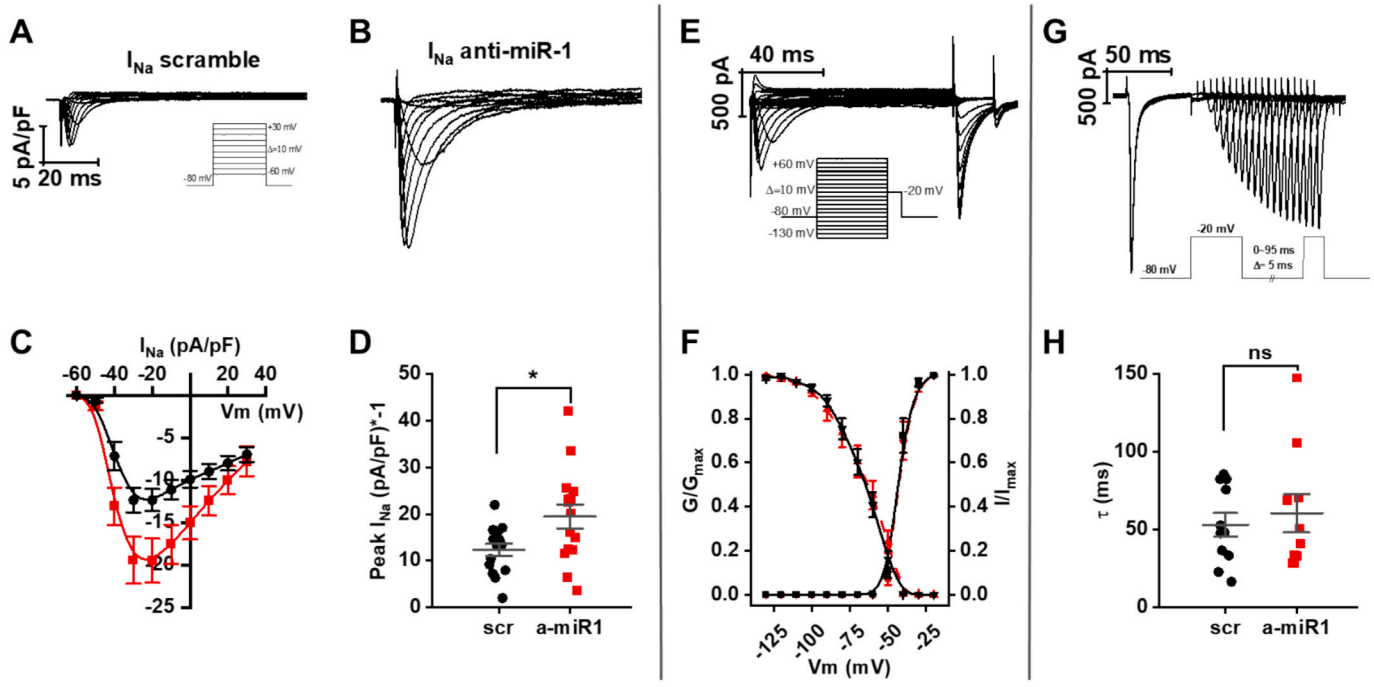

Fig. 4. Effect of anti-miR-1 oligonucleotide treatment on voltage-gated I_{Na} in iPSC-CM. (A) Typical I_{Na} trace of a cell transfected with the control oligonucleotide and (B) with the anti-miR-1 oligonucleotide. (C) I-V curves of the voltage-gated sodium channel of control (scrambled, black dots) and anti-miR-1 oligonucleotide-treated iPSC-CM (anti-miR-1, red squares; $n = 15$ for each group; error bars indicate SEM). (D) Scatter plot showing the quantification and comparison of both peak current densities, horizontal lines indicate the mean ± SEM (n = 15 for both groups; *p<0.05). (E) Representative I_{Na} traces of the two-pulse test to measure activation and inactivation kinetics. The inset shows the stimulus protocol. (F) Activation ($n = 12$) and inactivation ($n = 14$) curves of the voltage-gated sodium channel of iPSC-CM transfected with the negative control (black) and the anti-miR-1 oligonucleotide (red), respectively. (G) Representative current traces of the two-pulse test to investigate I_{Na} recovery kinetics. The inset shows the stimulation protocol. (H) Scatter plot showing the recovery time constant τ of the two groups, horizontal lines indicate the mean ± SEM ($n = 11$ for the scrambled, and $n = 10$ for the anti-miR-1 groups, respectively; no significant difference between the two groups). (For interpretation of the references to color in this figure legend, the reader is referred to the web version of this article.)

functionally active Na^+ channels at the sarcolemma as a consequence of miR-1 inhibition and enhanced Cx43 expression.

The kinetics of steady-state inactivation (h_∞) and activation (m_∞) of Na^+ channels were investigated with a two-pulse step protocol (Fig. 4E). The peak current evoked by the second pulse was normalized to the maximum I_{Na} and plotted against the conditioning voltage of the pre-step to establish the inactivation curve (Fig. 4F). The peak currents evoked by the first pulse were also normalized to maximum I_{Na} and plotted against the voltage of the conditioning pulse to create the activation curve (Fig. 4F). A Boltzmann fit was employed to calculate the slope, half-activation and half-inactivation voltages. There were no significant differences between the anti-miR-1 and control oligonucleotide-treated group regarding the half-activation and half-inactivation voltages. The results are summarized in Table 1.

Another two-pulse test was conducted to investigate the recovery kinetics of the voltage-dependent Na^+ channel, in which the time interval between two pulses increased step by step (Fig. 4G). The peak current intensity of the second pulse was divided by the peak of the first pulse and then plotted against the time interval between the two pulses. An exponential curve was fitted to calculate the recovery time constant (τ). There was no significant difference in the recovery time constant between the anti-miR-1 oligonucleotide treatment group and the control group (control: 53.1 ± 7.5 ms vs. anti-miR-1: 60.6 ± 12.4 ms; Fig. 4H).

3.5. Inhibition of miR-1 significantly influenced AP properties in iPSC-CM

We used the current clamp technique to record APs from single iPSC-CM to investigate the regulatory effect of miR-1. A series of stimuli with increasing intensity (i.e., input current amplitude) was applied to find the cell threshold to elicit an AP (Supplemental Fig. 8). Subsequently, a supra-threshold current stimulation protocol of 2 Hz was used to stimulate iPSC-CM. Typical traces of evoked APs of iPSC-CM transfected with scrambled or anti-miR-1 oligonucleotides are summarized in Fig. 5A. The resting membrane potential of the anti-miR-1 oligonucleotide-treated group was significantly lower than the control oligonucleotide-treated group (−58.2 ± 1.1 mV in control vs. –62.0 ± 1.1 mV in anti-miR-1-treated cells; n = 14 and 18; Fig. 5B). To characterize the dynamics of the initial phase of the AP, we used the peak value of the first derivative of phase 0 of the AP to determine the maximum upstroke velocity (dV/dt_{max}) (Fig. 5C). The results demonstrate that dV/dt_{max} of iPSC-CM transfected with the anti-miR-1 oligonucleotide was significantly increased compared to cells treated with the control oligonucleotide (21.2 ± 7.3 V/s in control vs. 43.4 ± 5.2 V/s in anti-miR-1-treated cells, Fig. 5D), suggesting higher excitability due to more functional $Na_v1.5$ channels at the membrane. Analysis of the action potential duration (APD) revealed no significant differences in control and anti-miR-1-treated cells (Supplemental Fig. 9).

3.6. Inhibition of miR-1 significantly synchronized field potentials in iPSC-CM

The electrical activity of iPSC-CM in monolayer cultures was assessed by MEA to investigate and record spontaneous field potentials generated by the cells. We validated the experimental setup using HL-1 cells. After a period of baseline stabilization, 30–60 s of spontaneous field potentials were recorded (upper trace in Fig. 6A). Data were analyzed using the OriginPro software. The spike interval was 2230 ± 172 ms, and the coefficient of variation (CoV) of the intervals was 0.24 ± 0.03 for HL-1 cells (n = 10). The beating frequency was 0.52 ± 0.06 Hz, with a CoV of the beat-to-beat frequency of 0.37 ± 0.01 for HL-1 cells (n = 10). These pilot data are summarized in Fig. 6B, D (in green).

Next, the effect of anti-miR-1 oligonucleotide treatment on iPSC-CM field potentials was assessed. Spontaneous electrical activity was recorded in control and anti-miR-1-treated cells, and the results revealed notable differences both in frequency and rhythmicity. Representative sample traces of 20 s recordings are illustrated in the center and bottom traces of Fig. 6A, revealing slow and irregular spontaneous electrical activity in control cells, whereas anti-miR-1-treated iPSC-CM presented fast and regular field potentials. The spike interval of the field potentials and the CoV of the intervals were significantly reduced in the anti-miR-1-treated compared to the control cells (mean interval in control: 522 ± 14 ms, n = 12, vs. 380 ± 7 ms in anti-miR-1, n = 11; CoV of interval in control: 0.36 ± 0.01 vs. 0.27 ± 0.02 in anti-miR-1, Fig. 6B, C). In addition, anti-miR-1 treatment significantly increased the beating frequency of iPSC-CM (from 2.3 ± 0.06 Hz in control, n = 12, to 2.9 ± 0.05 Hz in anti-miR-1, n = 11) while it decreased the CoV of frequency (from 0.30 ± 0.01 in control to 0.22 ± 0.01 in anti-miR-1; Fig. 6D, E). These results demonstrate that inhibition of miR-1 leads to significantly higher frequency, regularity and reduced variability of spontaneous APs, suggesting a high degree of temporally synchronized depolarization and strong electrical coupling across the cell monolayer, a combined beneficial effect of higher Cx43 expression and increased cell excitability through enhanced $Na_v1.5$ function.

Table 1
Steady-state activation and inactivation parameters of $Na_v1.5$ channels.

	Half-inactivation voltage (mV)	Slope of inactivation curve	Half-activation voltage (mV)	Slope of activation curve
anti-miR-1 (n = 12)	−62.3 ± 2.0	13.6 ± 1.9	−42.6 ± 0.2	2.9 ± 0.1
scrambled (n = 14)	−64.3 ± 1.1	11.2 ± 1.0	−43.1 ± 0.1	3.1 ± 0.1

4. Discussion

4.1. Increased Cx43 expression by miR-1 inhibition

The development of arrhythmogenic signals involves lateralization and reduced expression of Cx43 as well as diminished $Na_v1.5$ function, resulting in low intercellular coupling, decreased membrane excitability, and slowed impulse propagation in iPSC-CM [23]. Additionally, weak coupling increase the likelihood of uncoordinated excitation patterns and conduction barriers, which are potential mechanisms underlying arrhythmias [7]. This project aimed at identifying and characterizing new molecular targets to modulate Cx43 expression and membrane excitability in iPSC-CM, with the goals of (i) enhancing our understanding of disease progression and (ii) identifying novel therapeutic targets for idiopathic arrhythmias.

Experimental assays to modulate miR-1 activity were initially developed and optimized in HL-1 cells. After developing a modified μCP technique, we analyzed Cx43 expression in HL-1 and iPSC-CM cell strands. Although native Cx43 expression in HL-1 cells and iPSC-CM is relatively low, as demonstrated by our group and others [17], treatment with anti-miR-1 oligonucleotides significantly increased Cx43 protein levels, both in the perinuclear region and at the cell borders. Chronic stress induced by tachypacing resulted in a significant decrease in sarcolemmal Cx43 expression, which was restored by miR-1 inhibition even under stress conditions. Under these circumstances, the Cx43 distribution pattern resembled the one observed with experimentally increased Cx43 expression [18]. These new findings demonstrate a direct correlation between Cx43 expression levels and miR-1 activity, a micro-RNA that is highly abundant in developing murine cardiomyocytes [24]. The reduction in Cx43 expression observed during chronic stress is consistent with previous data showing that oxidative stress caused by tachypacing increases miR-1 expression while decreasing Cx43 protein levels in H_2O_2-treated cardiomyocytes [25]. Elevated miR-1 activity thus contributes to reduced Cx43 expression and impaired cell-cell coupling in iPSC-CM, whereas miR-1 inhibition directly enhances Cx43 expression and with it, the formation of hemichannels as well as gap junctions for intercellular communication.

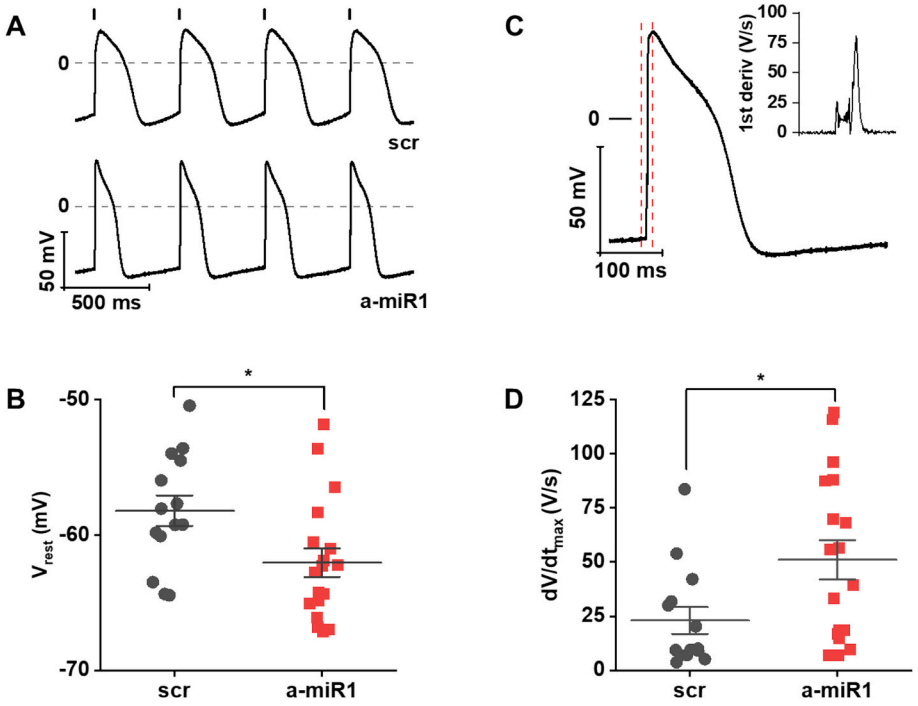

Fig. 5. Effect of miR-1 inhibition on APs of iPSC-CM. (A) APs of control (scrambled) and anti-miR-1 oligonucleotide-treated cells were evoked by a series of stimuli at 2 Hz pacing frequency, indicated by the upper stimulation indicators; the lower panels show the membrane potential. (B) Comparison of the resting membrane potential between control ($n = 14$) and anti-miR-1-treated iPSC-CM ($n = 18$). (C) shows a typical triggered AP of an anti-miR-1 oligonucleotide-treated iPSC-CM and its corresponding 1st derivative of phase 0 in the inset. The dashed area in red indicates the range for measuring the upstroke velocity. Please note the stimulus artefact. (D) Comparison of the upstroke velocity (dV/dt_{max}) between control and anti-miR-1-treated iPSC-CM (scramble: n = 14, anti-miR-1: n = 18). Data are shown as mean ± SEM; $^*p < 0.05$. (For interpretation of the references to color in this figure legend, the reader is referred to the web version of this article.)

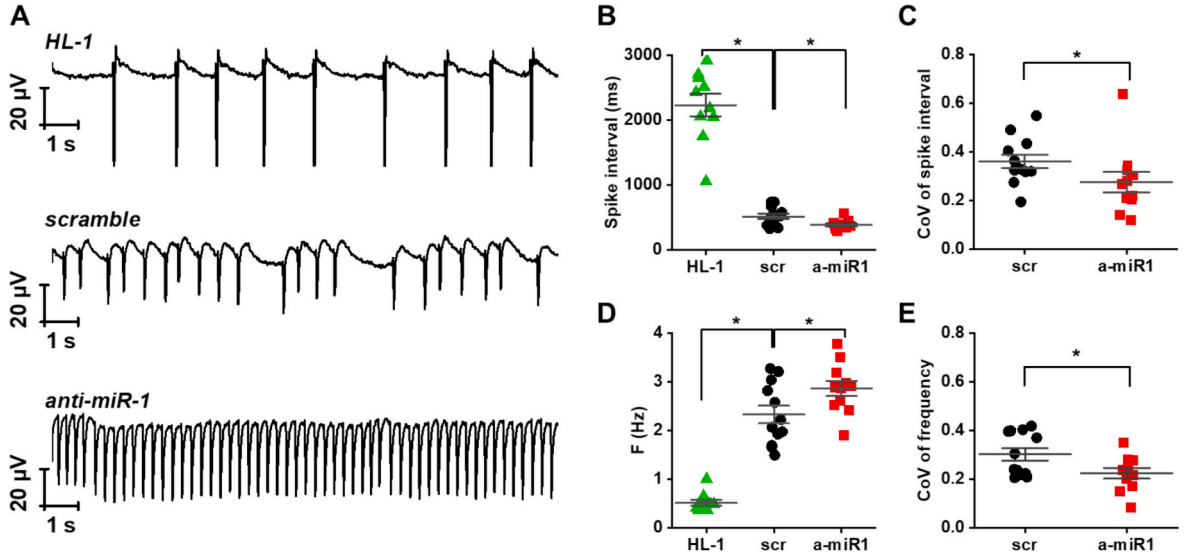

Fig. 6. Effect of miR-1 inhibition on spontaneous field potentials in HL-1 and iPSC-CM. (A) Field potential recordings of 20 s of HL-1 cells (top trace), control iPSC-CM (center trace) and anti-miR-1-treated iPSC-CM (bottom trace). (B) Comparison of the spike intervals of field potentials in HL-1 cells ($n = 10$), control ($n = 12$) and anti-miR-1-treated iPSC-CM ($n = 11$). (C) Comparison of CoV of the spike interval between control (n = 12) and anti-miR-1-treated iPSC-CM (n = 11). (D) Comparison of the beating frequencies of HL-1 cells (n = 10), control (n = 12) and anti-miR-1-treated iPSC-CM (n = 11). (E) CoV of frequency of control (n = 12) and anti-miR-1-treated iPSC-CM (n = 11). Each data dot represents the mean of 9 electrodes in one MEA chamber. One-way ANOVA revealed significantly different means ($^*p < 0.05$). (For interpretation of the references to color in this figure, the reader is referred to the web version of this article.)

Post-transcriptional regulation of Cx43 is mediated through the modulation of its mRNA stability and translation. The 3′s-UTR of Cx43 mRNA contains two binding sites for miR-1, both of which are essential for efficient downregulation of Cx43 translation [26]. Based on our findings, we propose a miR-1-dependent mechanism regulating Cx43 expression, wherein miR-1 mediates post-transcriptional gene silencing by binding to complementary sequences in the Cx43 mRNA. Tachypacing increases miR-1 activity through reactive oxygen species (ROS)-dependent signaling pathways, with the consequence of inhibiting the translation of Cx43 mRNA [14]. The introduction of anti-miR-1

oligonucleotides neutralized miR-1 activity via base-complement binding, effectively lifting its inhibitory effect on Cx43 translation. Consequently, more Cx43 protein was translated and transported to the sarcolemma, where it formed more hemichannels and functional gap junctions. In a clinical trial, Noorman et al. observed reduced Cx43 expression accompanied by increased miR-1 levels in patients with arrhythmogenic diseases [7]. Thus, miR-1 inhibition holds promise as a novel therapeutic approach for arrhythmias.

miR-1 is one of the most conserved miRNAs, specifically expressed in muscle tissue and implicated in a wide range of biological roles. Despite its highly specific effect on Cx43 mRNA, this is not its sole target [27,28]. miR-1 is also known to regulate various cellular processes, including proliferation, differentiation, and cardiomyocyte growth [29], and it may also influence protein phosphorylation in cardiomyocytes [30]. Therefore, future studies should carefully evaluate potential additional effects of miR-1-mediated interactions with other cardiac proteins and ion channels in iPSC-CM.

4.2. Enhanced cell membrane excitability after miR-1 inhibition

Intercellular coupling relies on multiple factors, with both intercellular resistance and excitability playing crucial roles in electrical signal propagation [31]. Membrane excitability primarily depends on the expression and availability of the fast voltage-gated Na^+ channels $Na_v1.5$ at the sarcolemma, more specifically in the perinexus surrounding gap junction plaques. Channel availability and $Na_v1.5$ currents are not only influenced by the number of functional channels expressed but also by the resting membrane potential, which determines channel availability [32,33].

To investigate the role of miR-1 in regulating cell excitability, we built directly on our previous studies [18] and tested whether enhanced Cx43 expression after miR-1 inhibition directs voltage-gated $Na_v1.5$ channels toward the perinexus. So, we analyzed $Na_v1.5$ channels and their contribution to evoked APs in iPSC-CM as previously described [18]. Our findings reveal that cells transfected with anti-miR-1 oligonucleotides exhibited significantly larger peak I_{Na} densities. Additionally, current-clamp data disclose faster AP upstroke velocities and lower resting membrane potentials, leading to higher excitability in these cells. The discovery that inhibition of miR-1 leads to more negative resting membrane potentials confirms the notion that cardiomyocytes expressing plenty of Cx43 are strongly coupled to each other forming a functional syncytium. This provides electrical stability across the cell layers and helps prevent localized inhomogeneities in the resting membrane potential and even local depolarizations, which can be arrhythmogenic. Additionally, miR-1 may also influence Kir2.1 expression, responsible for the inward rectifier current, which modulates the resting membrane potential in adult cardiomyocytes [13]. It will be therefore very interesting to address the effect of miR-1 on Kir2.1 in iPSC-cardiomyocytes in future studies. Since Na^+ channel kinetics, such as activation and inactivation parameters and the recovery time constant, were not significantly affected by miR-1 inhibition, it is likely that the number of functional Na^+ channels at the membrane increased. These findings highlight the intricate interplay between cell-cell coupling (Cx43) and cell excitability ($Na_v1.5$ channels).

Recent studies, including our own, have highlighted the spatial proximity of $Na_v1.5$ and Cx43, providing compelling evidence of a functional link between these channels [34,35]. Specifically, Cx43 membrane expression appears to facilitate $Na_v1.5$ recruitment to the intercalated disc [18,36]. However, the precise molecular mechanisms driving this interaction remain unclear. One study proposed that miR-1 may influence cell excitability through Nedd4-2, a regulator of sarcolemmal ion channels in cardiomyocytes [37]. Another in vivo study suggested an inverse relationship between miR-1 expression and cardiac conduction disturbances in rat myocardium [13]. Our results, however, support an alternative hypothesis: Cx43 expression may act as an attractor for $Na_v1.5$ shuttling to the intercalated discs, as previously suggested [18,38].

In summary, we demonstrate that inhibiting miR-1 activity with specific antisense oligonucleotides enhances Cx43 expression, which in turn increases Na^+ channel expression and function at the sarcolemma, thereby improving cell excitability. This is evidenced by increased I_{Na} and faster AP upstroke velocities. Consequently, two key factors essential for electrical signal propagation – gap junction intercellular communication and cell excitability – were significantly improved following miR-1 inhibition. The final functional confirmation of enhanced intercellular coupling and membrane excitability comes from our MEA experiments, which show significantly faster and more regular spontaneous field potentials after miR-1 inhibition, as discussed below.

4.3. Micro-RNA-1-dependent beating frequency and arrhythmogenesis in iPSC-CM

MEAs offer a valuable, non-invasive, and physiologically relevant method for assessing the electrophysiological characteristics of cardiac cell models [39]. To evaluate the impact of miR-1 on the electrical activity of iPSC-CM, we recorded spontaneous field potentials using MEAs and analyzed key parameters of intrinsic electrical activity. Molecular inhibition of miR-1 resulted in notable improvements in the electrical properties of iPSC-CM, particularly in the frequency and regularity of recorded field potentials. These enhancements in rhythmicity were further corroborated by confocal live imaging analysis of Ca^{2+} transients, which revealed significantly faster and more consistent Ca^{2+} dynamics following miR-1 inhibition.

These findings suggest that miR-1 inhibition strongly and significantly enhances the electrical activity of multicellular iPSC-CM preparations. This improvement is likely due to enhanced cell coupling and increased cell excitability, enabling source pulses to propagate more rapidly and consistently across the cell layer. Factors influencing automaticity include the spontaneous depolarization rate during phase 4 of the AP and the difference between the maximum diastolic potential (MDP) and the threshold potential. Gradual attenuation of outward K^+ currents and activation of inward HCN-dependent funny currents (I_f) drive automated depolarization in phase 4 of the AP, as explained by the "membrane clock theory" [40]. While the spontaneous electrical activity of iPSC-CM is a hallmark of their naïve phenotype [18], the observed increases in frequency and regularity of spontaneous depolarizations suggest that miR-1 may also influence voltage-gated K^+ and HCN channels in iPSC-CM. Further research will be needed to explore this hypothesis.

Under pathophysiological conditions, miR-1 is highly expressed in individuals with coronary artery disease, and its overexpression in normal or infarcted rat hearts exacerbates arrhythmogenic changes [13]. Conversely, our study demonstrates that irregular APs and Ca^{2+} transients are significantly improved by miR-1 inhibition. These findings suggest that targeted miR-1 inhibition may reduce the risk of arrhythmogenesis and could represent a promising new strategy for the treatment of arrhythmias.

4.4. Role of miR-1 on Ca^{2+} transient propagation in iPSC-CM

Ca^{2+} transients are primarily generated by elementary Ca^{2+} release events from intracellular Ca^{2+} stores, particularly the sarcoplasmic reticulum, and triggered by membrane depolarization. These transients are best measured using the fast linescan mode of laser-scanning confocal microscopes, which provides detailed information about the spatiotemporal properties of Ca^{2+} release in cardiomyocytes. Like APs, Ca^{2+} transients propagate along cardiomyocytes, thereby serving as a surrogate of electrical signal propagation [41]. Unlike video-based methods [42], we utilized linescan imaging to calculate the velocity of Ca^{2+} transient propagation across multiple cells with high temporal resolution. For analysis, each linescan image was evenly divided into ten segments along the spatial axis, representing individual cells. The

activation time for each segment was recorded, establishing a function of conduction distance versus time. The slope of a linear regression fit was then calculated to determine the average conduction velocity.

In HL-1 cells, we recorded an extremely low conduction velocity for Ca^{2+} transients, consistent with previous reports using the MEA technique [43]. Given the low expression levels of Cx43 in HL-1 cells, this result was expected. Similarly, Ca^{2+} transient conduction velocity was analyzed in iPSC-CM in cell monolayers and cell strands. The values recorded from monolayers closely matched the AP conduction velocity (~55 μm/ms) of pure murine embryonic stem cell-derived cardiomyocytes measured by MEAs in a prior study by our team [16]. In contrast, Ca^{2+} transient conduction velocity was reduced in cell strands (~30 μm/ms), which might indicate a source-sink mismatch that may slow down signal propagation along the narrow cell strands in these preparations.

Our experiments further demonstrated that cells transfected with anti-miR-1 oligonucleotides exhibited significantly faster conduction velocities compared to control cells in monolayer preparations. This finding suggests that miR-1 inhibition improves Ca^{2+} transient propagation in iPSC-CM, likely due to enhanced gap junction-mediated intercellular communication. This improvement facilitates the intercellular exchange of small molecules, including ions. In cardiomyocytes, an AP is typically followed by a Ca^{2+} transient, so our results indirectly confirm that miR-1 inhibition positively influences electrical signal propagation in these cells. An interesting and still unresolved question concerns the existence and functional role of Cx43 hemichannels in cardiomyocytes, particularly in relation to Ca^{2+} handling [3]. Although Cx43 hemichannels have not yet been investigated in iPSC-cardiomyocytes, there is strong evidence supporting their involvement in shaping Ca^{2+} signals in ventricular cardiomyocytes. These hemichannels form large conductance channels with poor ion selectivity and permit the passage of various small molecules, including ATP, mRNA and mono- and divalent cations [44]. Consequently, hemichannel-mediated Ca^{2+} influx may influence or trigger spontaneous Ca^{2+} release events, potentially stabilizing or destabilizing intracellular Ca^{2+} dynamics, depending on the cell's baseline state. It would be particularly interesting to investigate Cx43 hemichannel function in our cell model, especially following miR-1 inhibition, when increased Cx43 translation and channel formation are expected to occur as seen from our data set.

The introduction of the simplified model to assess the conduction properties of iPSC-CM greatly streamlines the calculation of Ca^{2+} transient propagation rates. However, the method has limitations, and the results should be considered approximate estimates of the true conduction velocity. A recent study reported that the classic diabetes drug metformin also improves electrical signal conduction by down-regulating miR-1 activity [25]. This underscores the potential of miR-1 modulation as an effective therapeutic target for arrhythmias.

Despite the improvements, the conduction velocity in iPSC-CM following miR-1 inhibition remains much slower than that observed in primary cardiomyocytes, as demonstrated previously in neonatal rat ventricular myocytes [43]. This indicates that a combination of strategies may be necessary to further enhance electrical coupling in iPSC-CM.

4.5. Conclusion

Alterations in Cx43 expression and gap junction function contribute to the development of arrhythmogenic changes in the heart; however, the underlying molecular mechanisms driving these remodeling processes remain poorly understood. In this study, we investigated the role of miR-1-mediated regulation of Cx43 expression on the electrophysiological properties of iPSC-CM. Building on our previous work [14], which demonstrated that miR-1 levels increase under chronic stress conditions, significantly reducing Cx43 membrane expression and intercellular coupling, we show here for the first time that molecular suppression of miR-1 during stress using anti-miR-1 oligonucleotides markedly enhances Cx43 expression and gap junction formation. Furthermore, we demonstrate that increased Cx43 expression correlates with higher current densities of voltage-gated Na^{+} channels. As a result, cell-to-cell communication improves, cell excitability is enhanced, and intercellular coupling becomes more efficient. This leads to faster AP upstroke velocities and overall improved electrical activity, as evidenced by increased frequency and reduced beat-to-beat variability of field potentials. Given these multiple beneficial effects of miR-1 inhibition on the electrical properties of cardiomyocytes, miR-1 emerges as a promising and effective therapeutic target for mitigating arrhythmogenic remodeling processes in cardiomyocytes at the level of Cx43 expression and gap junction function, to restore intercellular communication, and ensure robust electrical signal propagation.

CRediT authorship contribution statement

Xijian Ke: Writing – review & editing, Writing – original draft, Methodology, Investigation, Funding acquisition, Formal analysis, Data curation. **Jonathan S. Baillie:** Writing – review & editing, Writing – original draft. **Enrico D. Lemma:** Writing – review & editing, Validation, Methodology, Investigation. **Martin Bastmeyer:** Writing – review & editing, Methodology. **Markus Hecker:** Writing – review & editing, Supervision. **Nina D. Ullrich:** Writing – review & editing, Writing – original draft, Visualization, Validation, Supervision, Software, Resources, Project administration, Methodology, Funding acquisition, Conceptualization.

Declaration of Generative AI and AI-assisted technologies in the writing process

The authors did not use generative AI or AI-assisted technologies in the development of this manuscript.

Funding

This work was supported by the German Research Foundation (DFG, UL 466/2-1 to NDU) and by the Elisabeth and Rudolf Hirsch funding (to NDU). XK was supported by the Heinz Götze Memorial Fellowship Program of the Athenaeum Foundation (HGMF scholarships) and by the Tongji Hospital Research Fund (2022hgry019). EDL was supported by the Italian Ministry for University and Research (Young Researchers - Seal of Excellence, CUP C83C22001250006).

Declaration of competing interest

None.

Acknowledgements

We thank Manuela Höfer, Dr. Irene C. Marcu and Dr. Sarah Bertels for their excellent technical and experimental support.

Appendix A. Supplementary data

Supplementary data to this article can be found online at https://doi.org/10.1016/j.yjmcc.2025.05.008.

Data availability

All original data acquired for this study are available upon request.

References

[1] A. Di Marco, E. Claver, I. Anguera, Impact of cardiac magnetic resonance to arrhythmic risk stratification in nonischemic cardiomyopathy, Card. Electrophysiol. Clin. 15 (3) (2023) 379–390.

[2] D. Muser, P. Santangeli, J.J. Liang, Mechanisms of ventricular arrhythmias and implications for catheter ablation, Card. Electrophysiol. Clin. 14 (4) (2022) 547–558.
[3] M.A.J. de Smet, A. Lissoni, T. Nezlobinsky, N. Wang, E. Dries, M. Pérez-Hernández, et al., Cx43 hemichannel microdomain signaling at the intercalated disc enhances cardiac excitability, J. Clin. Invest. 131 (7) (2021) e137752.
[4] A. Rodríguez-Sinovas, J.A. Sánchez, L. Valls-Lacalle, M. Consegal, I. Ferreira-González, Connexins in the heart: regulation, function and involvement in cardiac disease, Int. J. Mol. Sci. 22 (9) (2021) 4413.
[5] O.M. Rusiecka, J. Montgomery, S. Morel, D. Batista-Almeida, Campenhout R. Van, M. Vinken, et al., Canonical and non-canonical roles of connexin43 in cardioprotection, Biomolecules 10 (9) (2020) 1–22.
[6] P. Bedner, H. Niessen, B. Odermatt, K. Willecke, H. Harz, A method to determine the relative cAMP permeability of connexin channels, Exp. Cell Res. 291 (1) (2003) 25–35.
[7] M. Noorman, S. Hakim, E. Kessler, J.A. Groeneweg, M.G.P.J. Cox, A. Asimaki, et al., Remodeling of the cardiac sodium channel, connexin43, and plakoglobin at the intercalated disk in patients with arrhythmogenic cardiomyopathy, Hear. Rhythm. 10 (3) (2013) 412–419.
[8] E.T. Hoorntje, W.P. Te Rijdt, C.A. James, K. Pilichou, C. Basso, D.P. Judge, et al., Arrhythmogenic cardiomyopathy: pathology, genetics, and concepts in pathogenesis, Cardiovasc. Res. 113 (12) (2017) 1521–1531.
[9] J.F. Calderón, M.A. Retamal, Regulation of connexins expression levels by MicroRNAs, an update, Front. Physiol. 7 (2016) 558.
[10] M. Oyamada, K. Takebe, Y. Oyamada, Regulation of connexin expression by transcription factors and epigenetic mechanisms, Biochim. Biophys. Acta 1828 (1) (2013) 118–133.
[11] B. Bian, X.F. Yu, G.Q. Wang, T.M. Teng, Role of miRNA-1 in regulating connexin 43 in ischemia-reperfusion heart injury: a rat model, Cardiovasc. Pathol. 27 (2017) 37–42.
[12] H.F. Xu, Y.J. Ding, Y.W. Shen, A.M. Xue, H.M. Xu, C.L. Luo, et al., MicroRNA-1 represses Cx43 expression in viral myocarditis, Mol. Cell. Biochem. 362 (1–2) (2012) 141–148.
[13] B. Yang, H. Lin, J. Xiao, Y. Lu, X. Luo, B. Li, et al., The muscle-specific microRNA miR-1 regulates cardiac arrhythmogenic potential by targeting GJA1 and KCNJ2, Nat. Med. 13 (4) (2007) 486–491.
[14] C.M. Wahl, C. Schmidt, M. Hecker, N.D. Ullrich, Distress-mediated remodeling of cardiac connexin-43 in a novel cell model for arrhythmogenic heart diseases, Int. J. Mol. Sci. 23 (17) (2022) 10174.
[15] Y. Zhang, H. Wang, A. Kovacs, E.M. Kanter, K.A. Yamada, Reduced expression of Cx43 attenuates ventricular remodeling after myocardial infarction via impaired TGF-β signaling, Am. J. Physiol. Heart Circ. Physiol. 298 (2) (2010) H477–H487.
[16] J.P. Kucera, Y. Prudat, I.C. Marcu, M. Azzarito, N.D. Ullrich, Slow conduction in mixed cultured strands of primary ventricular cells and stem cell-derived cardiomyocytes, Front. Cell Dev. Biol. 3 (2015) 58.
[17] I.C. Marcu, A. Illaste, P. Heuking, M.E. Jaconi, N.D. Ullrich, Functional characterization and comparison of intercellular communication in stem cell-derived cardiomyocytes, Stem Cells 33 (7) (2015) 2208–2218.
[18] V. Sottas, C.M. Wahl, M.C. Trache, M. Bartolf-Kopp, S. Cambridge, M. Hecker, et al., Improving electrical properties of iPSC-cardiomyocytes by enhancing Cx43 expression, J. Mol. Cell. Cardiol. 120 (2018) 31–41.
[19] A. Körner, M. Mosqueira, M. Hecker, N.D. Ullrich, Substrate stiffness influences structural and functional remodeling in induced pluripotent stem cell-derived cardiomyocytes, Front. Physiol. 12 (2021) 1306.
[20] W.C. Claycomb, N.A. Lanson, B.S. Stallworth, D.B. Egeland, J.B. Delcarpio, A. Bahinski, et al., HL-1 cells: a cardiac muscle cell line that contracts and retains phenotypic characteristics of the adult cardiomyocyte, Proc. Natl. Acad. Sci. U. S. A. 95 (6) (1998) 2979–2984.
[21] R. Singhvi, A. Kumar, G.P. Lopez, G.N. Stephanopoulos, D.I.C. Wang, G. M. Whitesides, et al., Engineering cell shape and function, Science 264 (5159) (1994) 696–698.
[22] O.P. Hamill, A. Marty, E. Neher, B. Sakmann, F.J. Sigworth, Improved patch-clamp techniques for high-resolution current recording from cells and cell-free membrane patches, Pflugers Arch. 391 (2) (1981) 85–100.
[23] M. Paci, K. Penttinen, M. Pekkanen-Mattila, J.T. Koivumäki, Arrhythmia mechanisms in human induced pluripotent stem cell-derived cardiomyocytes, J. Cardiovasc. Pharmacol. 77 (3) (2020) 300–316.
[24] E.A. Alfar, A. El-Armouche, K. Guan, MicroRNAs in cardiomyocyte differentiation and maturation, Cardiovasc. Res. 114 (6) (2018) 779–781.
[25] L. Lv, N. Zheng, L. Zhang, R. Li, Y. Li, R. Yang, et al., Metformin ameliorates cardiac conduction delay by regulating microRNA-1 in mice, Eur. J. Pharmacol. 881 (2020) 173131.
[26] C. Anderson, H. Catoe, R. Werner, MIR-206 regulates connexin43 expression during skeletal muscle development, Nucleic Acids Res. 34 (20) (2006) 5863–5871.
[27] S. Ikeda, A. He, S.W. Kong, J. Lu, R. Bejar, N. Bodyak, et al., MicroRNA-1 negatively regulates expression of the hypertrophy-associated calmodulin and Mef2a genes, Mol. Cell. Biol. 29 (8) (2009) 2193–2204.
[28] K. Goljanek-Whysall, H. Pais, T. Rathjen, D. Sweetman, T. Dalmay, A. Münsterberg, Regulation of multiple target genes by miR-1 and miR-206 is pivotal for C2C12 myoblast differentiation, J. Cell Sci. 125 (Pt 15) (2012) 3590–3600.
[29] S. Paiva, O. Agbulut, MiRroring the multiple potentials of microRNAs in acute myocardial infarction, Front. Cardiovasc. Med. 4 (2017) 73.
[30] A.E. Belevych, S.E. Sansom, R. Terentyeva, H.T. Ho, Y. Nishijima, M.M. Martin, et al., MicroRNA-1 and -133 increase arrhythmogenesis in heart failure by dissociating phosphatase activity from RyR2 complex, PloS One 6 (12) (2011) e28324.
[31] A.G. Kléber, Q. Jin, Coupling between cardiac cells—an important determinant of electrical impulse propagation and arrhythmogenesis, Biophys. Rev. 2 (3) (2021) 031301.
[32] B.C. Eloff, D.L. Lerner, K.A. Yamada, R.B. Schuessler, J.E. Saffitz, D.S. Rosenbaum, High resolution optical mapping reveals conduction slowing in connexin43 deficient mice, Cardiovasc. Res. 51 (4) (2001) 681–690.
[33] S. Weidmann, The effect of the cardiac membrane potential on the rapid availability of the sodium-carrying system, J. Physiol. 127 (1) (1955) 213–224.
[34] J.M. Rhett, E.L. Ongstad, J. Jourdan, R.G. Gourdie, Cx43 associates with Nav1.5 in the cardiomyocyte perinexus, J. Membr. Biol. 245 (7) (2012) 411–422.
[35] R. Veeraraghavan, G.S. Hoeker, A.A. Laviada, D. Hoagland, X. Wan, D.R. King, et al., The adhesion function of the sodium channel beta subunit (β1) contributes to cardiac action potential propagation, Elife (2018) 7.
[36] E. Agullo-Pascual, M. Cerrone, M. Delmar, Arrhythmogenic cardiomyopathy and Brugada syndrome: diseases of the connexome, in: FEBS Letters, FEBS Lett, 588, 2014, pp. 1322–1330.
[37] J.Y. Zhu, A. Heidersbach, I.S. Kathiriya, B.I. Garay, K.N. Ivey, D. Srivastava, et al., The E3 ubiquitin ligase Nedd4/Nedd4L is directly regulated by microRNA 1, Development 144 (5) (2017) 866–875.
[38] E. Agullo-Pascual, X. Lin, A. Leo-Macias, M. Zhang, F.X. Liang, Z. Li, et al., Super-resolution imaging reveals that loss of the C-terminus of connexin43 limits microtubule plus-end capture and NaV1.5 localization at the intercalated disc, Cardiovasc. Res. 104 (2) (2014) 371–381.
[39] J. Hescheler, M. Halbach, U. Egert, Z.J. Lu, H. Bohlen, B.K. Fleischmann, et al., Determination of electrical properties of ES cell-derived cardiomyocytes using MEAs, J. Electrocardiol. 37 (SUPPL) (2004) 110–116.
[40] D. DiFrancesco, A brief history of pacemaking, Front. Physiol. 10 (2020).
[41] Q. Jin, K.Y. Lee, Z. Selimi, D. Shimura, E. Wang, J.F. Zimmerman, et al., Determinants of electrical propagation and propagation block in arrhythmogenic cardiomyopathy, J. Mol. Cell. Cardiol. 186 (2024) 71–80.
[42] A.P. Petersen, N. Cho, D.M. Lyra-Leite, J.W. Santoso, D. Gupta, N.R. Ariyasinghe, et al., Regulation of calcium dynamics and propagation velocity by tissue microstructure in engineered strands of cardiac tissue, Integr. Biol. (Camb). 12 (2) (2020) 34–46.
[43] S.P. Wells, H.M. Waddell, C.B. Sim, S.Y. Lim, G.B. Bernasochi, D. Pavlovic, et al., Cardiomyocyte functional screening: interrogating comparative electrophysiology of high-throughput model cell systems, Am. J. Physiol. Cell Physiol. 317 (6) (2019) C1256–C1267.
[44] L. Leybaert, M.A.J. De Smet, A. Lissoni, R. Allewaert, H.L. Roderick, G. Bultynck, et al., Connexin hemichannels as candidate targets for cardioprotective and anti-arrhythmic treatments, J. Clin. Invest. 133 (6) (2023) e168117.